Optically pumped distributed feedback dye lasing with slide-coated TiO₂ inverse-opal slab as Bragg reflector

Sung Gu Han,[1,†] Jongchul Lim,[2,†] Jinsub Shin,[1] Sung-Min Lee,[3] Taiho Park,[2] Jongseung Yoon,[3] Kyoungja Woo,[4] Hyunjung Lee,[5] and Wonmok Lee[1,*]

[1]Department of Chemistry, Sejong University, Gwngjin-gu, Seoul 143-747, South Korea
[2]Department of Chemical Engineering, Pohang University of Science and Technology, Pohang 790-784, South Korea
[3]Department of Chemical Engineering and Materials Science, University of Southern California, Los Angeles, California 90089, USA
[4]Korea Institute of Science and Technology, Hwarangno Seoul, 136-792, South Korea
[5]School of Advanced Materials Engineering, Kookmin University, Seoul, 136-702, South Korea
*Corresponding author: wonmoklee@sejong.ac.kr

We demonstrate an optical amplification of organic dye within a TiO₂ inverse-opal (IO) distributed feedback (DFB) reflector prepared by a slide-coating method. Highly reflective TiO₂ IO film was fabricated by slide coating the binary aqueous dispersions of polystyrene microspheres and charge-stabilized TiO₂ nanoparticles on a glass slide and subsequently removing the polymer-opal template. TiO₂ IO film was infiltrated, in turn, with the solutions of DCM, a fluorescent dye in various solvents with different indices of refraction. Optical pumping by frequency-doubled Nd: YAG laser resulted in amplified spontaneous emission in each dye solution. In accordance with the semi-empirical simulation by the FDTD method, DCM in ethanol showed the best emission/stopband matching for the TiO₂ IO film used in this study. Therefore, photo excitation of a DCM/ethanol cavity showed a single-mode DFB lasing at 640 nm wavelength at moderate pump energy.   © 2014 Optical Society of America

OCIS codes: (140.3490) Lasers, distributed-feedback; (250.7260) Vertical cavity surface emitting lasers; (350.3390) Laser materials processing; (160.5298) Photonic crystals.
http://dx.doi.org/10.1364/OL.39.004743

Since the first introduction of photonic crystal (PhC) by Yablonovitch [1], there has been comprehensive research on on-chip integration of PhC devices that can realize various ways of light modulation such as confining [2], bending [3], amplifying [4], and stopping [5] of light within dielectric media having periodic structures. As a unique application for PhC in active mode, microlaser has been one of the hottest topics among PhC devices, since it generates the coherent beam within an extremely small volume. PhC laser action can occur in either defect mode or band-edge mode. There have been successful demonstrations of microlasers using one-dimensional (1D) and two-dimensional (2D) PhC [4,6,7]. In particular, low-threshold microlasers using PhC as 1D Bragg reflectors have been successfully demonstrated in-step with recent developments in materials synthesis and fabrication techniques [8,9]. From a practical standpoint, well-ordered self-assembly structures, such as face-centered cubic (FCC) colloidal crystals and microphase-separated block copolymers (BCP), are often considered to be attractive candidates for a PhC platform in comparison to those from top-down lithographic techniques due to the fast and easy processes used to form a large-area PhC template. Yoon and Thomas demonstrated an optically pumped defect-mode microlaser by using 1D lamellar BCP self-assembly as the Bragg reflector [10]. Shkunov and co-workers utilized silica opal as a self-assembled distributed feedback (DFB) reflector for random- [11] and single-mode lasing [12]. They demonstrated that single crystalline FCC opal can amplify photoluminescence (PL) along three different crystalline facets when infiltrated with different dyes for bandgap matching [12]. Lasing at the edge of the photonic stopband of

cholesteric liquid crystals has also been reported [13]. In spite of successful applications of the self-assembled PhC structures as Bragg reflectors, the synthesis or fabrication techniques to obtain PhC structures were too difficult and time consuming in the above studies (e.g., anionic polymerization of a BCP, growth of a single crystalline opal), and thus remain the points at issue. Recently, Kim *et al.* demonstrated low-threshold dye lasing using polymer/silica composite film and polymeric inverse opal (IO) film as Bragg reflectors templated by silica opal [14]. Nishijima *et al.* showed a cavity-mode dye laser within silica IO structure [15]. In a recent publication, we reported a facile route to obtain highly reflective TiO₂ IO film through an evaporation-induced planar coating of binary colloidal dispersion followed by thermal calcination [16]. The resulting TiO₂ IO film typically showed a bright reflective color that can be tuned by changing the colloidal particle size. The use of TiO₂ as a Bragg reflector can bring about strong optical resonance due to its high refractive index (>2.0). In the present study, a state-of-the-art application of TiO₂ IO film as a Bragg reflector for optically pumped DFB lasing is demonstrated. TiO₂ IO film was prepared through a slide-coating method in which binary aqueous dispersions of the negatively charged polystyrene (PS) microspheres and the anatase TiO₂ nanoparticles with respective particle sizes of 300 and 20 nm form a thin film of well-ordered PS opals with TiO₂ nanoparticles filled in the interstitial space. The particle sizes of PS microspheres and TiO₂ nanoparticles were engineered for the stopband edge of the IO cavity to be matched with the PL wavelength of the active medium. The synthetic procedures for the materials can be found elsewhere [17,18].
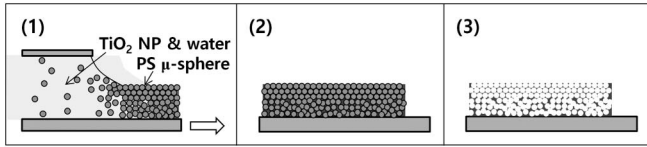
Fig. 1. Fabrication procedures for TiO$_2$ IO reflector by (1) slide coating an aqueous mixture of PS and TiO$_2$ particles, (2) drying the binary opal, and (3) removing the PS opal template.

For the preparation of IO film, a modified slide-coating technique has been applied [16]. Experimental variables for coating the solid contents in the colloidal dispersions or the coating speeds were carefully optimized to result in a 10 μm-thick IO film on a glass slide. The coated binary colloidal film was calcined in a furnace at 450° C to remove the PS opal template (Fig. 1).

The resulting TiO$_2$ IO film on a glass slide was assembled to create a cavity by gluing three pieces of glass wall together and adding a cover slide on top of it. The completed 1 mm-thick cavity was filled with dye solution. 10^{-3} M solutions of 4-dicyano-methylene-2-methyl-6-4-dimethyl-aminostyryl-4H-pyran (DCM, Exciton) in various solvents were prepared as the active PL emitters, among which a DCM/ethanol (EtOH) turned out to be the best choice for stopband matching. In Fig. 2(a), a schematic of a laser cavity with an optical pumping experiment is shown.

A frequency-doubled Nd:YAG pulsed laser with a repetition rate of 10 Hz and pulse duration of 7 ns was used as a pumping source. The as-prepared TiO$_2$ IO film exhibited a bright green reflective color at normal incidence of room light, as shown in the inset figure of Fig. 2(b), originating from Bragg diffraction of light from well-ordered periodic IO structure; as shown in Fig. 2(b), a tilted view of an SEM image of a TiO$_2$ IO film. The top surface of the IO film shows that the original PS particles had been closely packed during the slide-coating process with the sintered TiO$_2$ nanoparticles forming the IO skeleton. When the IO film was seen from the bottom, no structural color was observed due to a lack of long-range order. In spite of poor ordering at the bottom, the reflectance from the well-ordered upper layers at the stopband position was high (>40%) enough to amplify the emitted light along the perpendicular direction of a substrate surface. λ_{stop}, the stopband wavelength of the IO film at normal

incidence of light, can be simply estimated by using a modified Bragg equation for FCC lattice, as shown by Eq. 1 [19]:

$$\lambda_{stop} = (8/3)^{1/2}(p/m) \cdot (f_{pore} \cdot n_{pore}^2 + f_{TiO_2} \cdot n_{TiO_2}^2)^{1/2}$$
$$= 1.633 \cdot p \cdot n_{eff}, \tag{1}$$

where p is the periodic distance between IO pores; m is the order of the Bragg diffraction; and n_{pore}, n_{TiO_2}, f_{pore}, and f_{TiO_2} are the refractive indices (n) and the filling factors (f) of the pores and TiO$_2$, respectively. For an FCC IO structure in EtOH, one can roughly estimate n_{eff} as ~1.8, assuming $n_{TiO_2} = 2.0$ and $f_{pore} = 0.74$ (a filling factor of FCC lattice). However, an actual f_{pore} of a TiO$_2$ IO film is expected to be larger than 74% due to the volume shrinkage of TiO$_2$ during thermal calcination [16]. For more rigorous physical characterization of the TiO$_2$ IO film taking the aforementioned structural characteristics into account, finite-difference time domain (FDTD) simulations were carried out, from which the theoretical reflectances of the TiO$_2$ IO film consisting of 30-layer stacks of FCC (111) planes were obtained. The spectroscopic n_{TiO_2} and molar extinction coefficient (k) of a thin spin-coated TiO$_2$ film were obtained by ellipsometry (Nanoview), and these data were directly used for FDTD calculations. To simplify the calculation, a fixed n_{pore} was applied as a nonabsorbing liquid in pores (e.g., 1.36 for EtOH). To vary f_{TiO_2} in the simulation, we used the ratio D/p, where D is the diameter of the pore. As defined in Eq. 1, p stands for the average distance between pores, which is measured to be 283 nm from an SEM image, as shown in Fig. 3(a). Since we used PS microspheres with
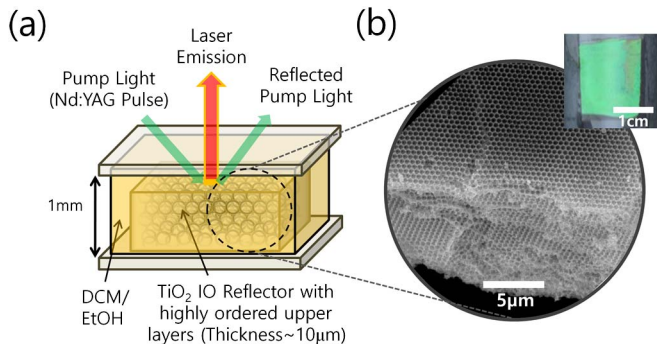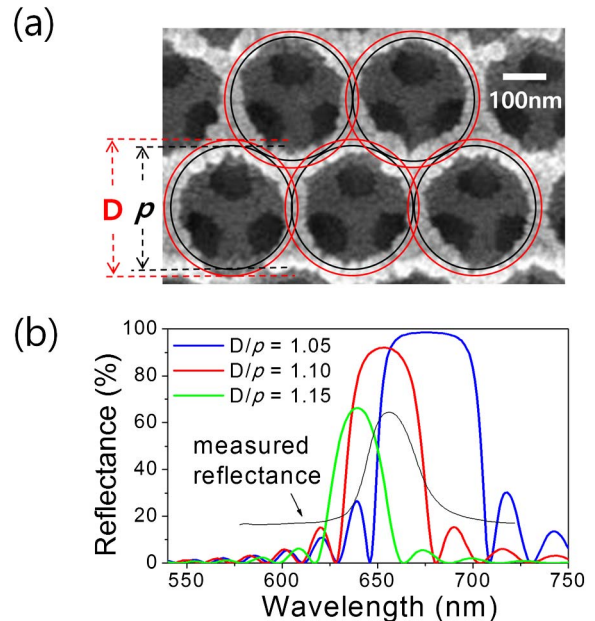

Fig. 2. (a) Schematic representation of a laser cavity and PL experiment. (b) SEM image of TiO$_2$ IO reflector showing a top surface and a cross-section of highly ordered IO structure. Inset shows a reflective color of TiO$_2$ IO film.

Fig. 3. (a) Magnified SEM image of a TiO$_2$ IO film on which period size p and diameter D of pore are drawn. From the SEM image, p is measured to be 283 nm and D is a variable for the calculation. In the figure, a D/p of 1.1 is shown. (b) FDTD simulation results with three D/p values. The measured reflectance spectrum is overlaid for comparison with the FDTD simulation.

300 nm diameter for opal templating, the measured p (283 nm) implies that there has been 5.7% lateral shrinkage in the TiO_2 film during thermal treatment induced by dehydration of TiO_2 nanoparticles and the removal of organic residues. In the simulation, D/p was varied from 1.05 to 1.15 with an assumption that thermal sintering of TiO_2 reduces the filling factor as well. An increase in D/p implies a growing pore size at a fixed p to result in a decrease in f_{TiO_2}. Figure 3(a) depicts two circles (D and p) with D/p of 1.1, for example, where the pore size D is 10% larger than that of p. In Fig. 3(b), the simulated reflectance spectra with three different D/p values are overlaid. The peak reflectances of all three simulations are higher than those of the measured reflectance, as shown in Fig. 3(b), since the perfect FCC structures are assumed in the modeled calculation, which is not true for our IO sample. With increases in D/p, the simulations tend to show the lowering and narrowing of the stopband peaks as well as the shifting toward shorter wavelength due to the decreases in f_{TiO_2}. Comparing the FDTD simulation results with the measured spectrum, it is reasonable to conclude that D/p would be close to 1.1 and the f_{TiO_2} less than 0.26.

To obtain an amplified emission from a DCM emitter in a given DFB system, the spectral position of the Bragg reflector's stopband edge must be properly matched with the maximum PL wavelength of the emitter. At the stopband edge, the group velocity of photons of the corresponding wavelength is minimized within the DFB structure, and subsequent enhancement of spontaneous emission occurs while those of other wavelengths get suppressed [10]. Therefore, fine-tuning of the stopband position is as important as structural perfection of the IO reflector to achieve a laser action. In fabrication of the DFB reflector via colloidal templating, the stopband position of an IO reflector can be systematically tuned by n variations. Tuning can be experimentally done by selecting the organic solvent for DCM with appropriate n. In this regard, toluene, DMF, and EtOH were chosen for candidates, which are in decreasing order of n, and the consecutive FDTD calculations were carried out using different n_{pore} values, which correspond to n values of the respective solvents ($n_{toluene} = 1.49$, $n_{DMF} = 1.435$, and $n_{EtOH} = 1.36$). The resulting reflectance spectra were compared with the measured spectra in the respective organic solvents. It was confirmed that the simulated stopband positions are in good accordance with the measured spectra. Comparison showed that TiO_2 IO film in EtOH has the best stopband matching with the DCM's PL maxima. In Fig. 4, the optically pumped PL spectra of DCM-containing TiO_2 IO cavities filled with respective solvents are shown. A frequency-doubled Nd:YAG pulsed laser ($\lambda_{max} = 532$ nm) was used as the excitation source for each cavity, and the pump energies were controlled by using a series of neutral-density filters (Edmund Optics). The emitted PLs from the excited spots were collected by a photon detector (iStar-DH734, Andor) with a time-resolved emission decay system that was specially installed using a pulse delay-generator (DG535) to control the photon detector at the exact moment of lasing action.

The Δn in Figs. 4(a)–4(c) are the calculated refractive index contrasts between TiO_2 IO and the respective
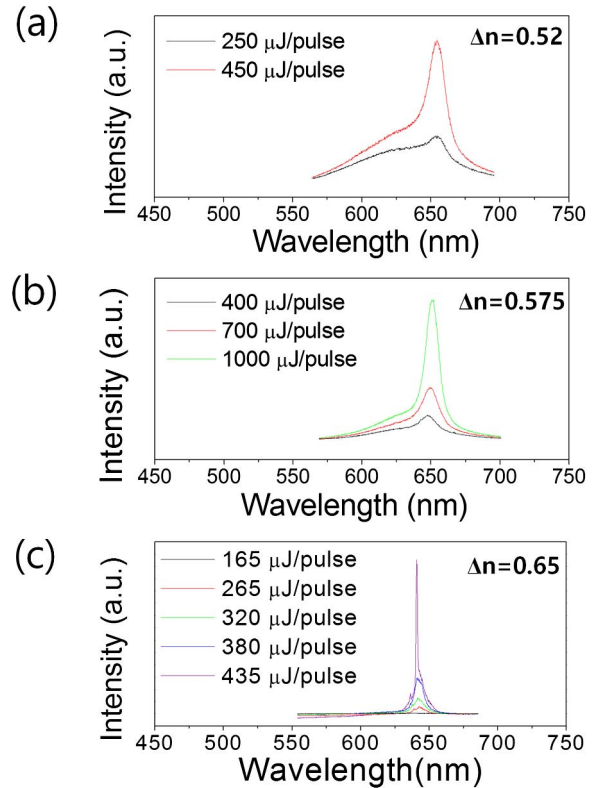

Fig. 4. Optically pumped PL spectra of DCM within TiO_2 IO DFB reflector using (a) Toluene, (b) DMF, and (c) EtOH as solvent for DCM where the wavelength shifts in ASE in each solvent are evident. Δn in each spectrum stands for the index contrast between TiO_2 IO and the respective solvent at 650 nm.

solvents at 650 nm, which are important properties for strong optical resonance. It is noteworthy that all three cavities show the amplified spontaneous emission (ASE) on top of the broad PL spectra. To make sure that those peaks are from ASE, a TiO_2 film with randomly oriented pores was prepared, and it was confirmed that optical pumping of DCM/toluene in the presence of this TiO_2 reflector shows no ASE at pump energy as high as 1.5 mJ. Despite the well-ordered IO structure exhibited at an ASE in DCM/toluene solution, as shown in Fig. 4(a), lasing was not observed due to a slight mismatch of the stopband edge position with PL maxima of DCM. However, DCM solutions in DMF and EtOH, respectively, resulted in narrowing of ASE bandwidths along with suppression of the broad DCM emissions due to the improved stopband matching (Figs. 4(b) and 4(c)). The peak wavelengths (λ_{peak}) of the ASEs in the three respective solvents in decreasing order of n were observed at 655, 651, and 642 nm, respectively (Figs. 4(a)–4(c)). The corresponding full width at half-maximum (FWHM) of the respective ASEs were 20, 16, and 8 nm at the largest pump energy for each cavity, showing spectral narrowing of ASE through fine-tuning of the stopband positions. When DCM/EtOH cavity was pumped by 435 μJ pulse, a narrow-band surface-emitting laser action was observed at λ_{peak} of 640 nm with the FWHM of 1.5 nm. A nonlinear response of PL intensities at λ_{peak} from a DCM/EtOH cavity is plotted in Fig. 5 as a function of pump energy, from which the lasing threshold of
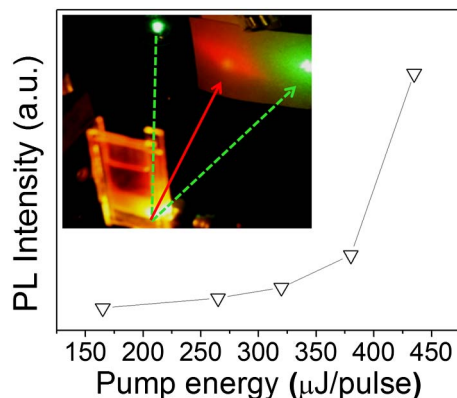
Fig. 5. Variation of PL intensities as a function of pump energy showing nonlinear increases of PL intensity at λ_{peak}. Inset figure shows a photograph of a laser cavity excited by pump light (green-dashed line) and a projected red lasing spot on a white screen (red solid line).

~350 µJ could be estimated. This threshold corresponds to ~3.5 MW/cm^2, which is comparable to those of previous investigations by silica opal templating [12,14]. In spite of poorly oriented bottom layers resulting in random light scattering within the cavity, a low threshold obtained in the slide-coated TiO$_2$ IO reflector can be attributed to a high refractive index of TiO$_2$. As shown in the upper-left inset of Fig. 5, the surface-emitting laser spot perpendicular to the reflector surface is shown as a red dot on a white screen since the amplification of the emission occurs only along the normal direction of FCC (111) planes.

In summary, we fabricated a highly reflective TiO$_2$ IO film by a simple slide coating of TiO$_2$ nanoparticle/PS microsphere binary opal film on a glass slide and a subsequent removal of PS templates by thermal calcination. The fabricated TiO$_2$ IO film showed a bright green reflective color, which was good enough for bandgap lasing of DCM in organic solvents. By optimizing the sacrificial particle size and the refractive index of the solvent for DCM, the edge wavelength of the stopband of TiO$_2$ IO film could be matched with PL wavelength of DCM. FDTD simulations of the optical reflectances from the TiO$_2$ IO film confirmed that the filling factor of TiO$_2$ in IO structure is less than 26%. When optically pumped with Nd:YAG pulsed laser, TiO$_2$ IO films in three solvents of Toluene, DMF, and EtOH, respectively, showed ASEs due to the light-trapping effect within the DFB structures. When the IO film was filled with EtOH, the best matching

between the stopband edge and the PL spectrum of DCM was achieved, and therefore a low-threshold single-mode DFB lasing could be obtained.

References

1. E. Yablonovitch, Phys. Rev. Lett. **58**, 2059 (1987).
2. J. D. Joannopoulos, R. D. Meade, and J. N. Winn, *Photonic Crystals: Molding the Flow of Light* (Princeton University, 1995).
3. S.-Y. Lin, E. Chow, V. Hietala, P. R. Villeneuve, and J. D. Joannopoulos, Science **282**, 274 (1998).
4. O. Painter, R. K. Lee, A. Scherer, A. Yariv, J. D. O'Brien, P. D. Dapkus, and I. Kim, Science **284**, 1819 (1999).
5. G. Pan, R. Kesavamoorthy, and S. A. Asher, Phys. Rev. Lett. **78**, 3860 (1997).
6. S. Noda, M. Yokoyama, M. Imada, A. Chutinan, and M. Mochizuki, Science **293**, 1123 (2001).
7. S. Noda, K. Tomoda, N. Yamamoto, and A. Chutinan, Science **289**, 604 (2000).
8. J. Yoon, W. Lee, J.-M. Caruge, M. Bawendi, E. L. Thomas, S. Kooi, and P. N. Prasad, Appl. Phys. Lett. **88**, 091102 (2006).
9. Y. Takeoka and M. Watanabe, Langmuir **18**, 5977 (2002).
10. J. Yoon, W. Lee, and E. L. Thomas, Nano Lett. **6**, 2211 (2006).
11. M. N. Shkunov, M. C. DeLong, M. E. Raikh, Z. V. Vardeny, A. A. Zakhidov, and R. H. Barughman, Synthetic Metals **116**, 485 (2001).
12. M. N. Shkunov, Z. V. Vardeny, M. C. DeLong, R. C. Polson, A. A. Zakhidov, and R. H. Baughman, Adv. Mater. **12**, 21 (2002).
13. V. I. Kopp, B. Fan, H. K. M. Vithana, and A. Z. Genack, Opt. Lett. **23**, 1707 (1998).
14. S. H. Kim, S. Kim, W. C. Jeong, and S. M. Yang, Chem. Mater. **21**, 4993 (2009).
15. Y. Nishijima, K. Ueno, S. Juodkazis, V. Mizeikis, H. Fujiwara, K. Sasaki, and H. Misawa, Opt. Express **17**, 2976 (2009).
16. Y. G. Seo, J. Woo, H. Lee, and W. Lee, Adv. Funct. Mater. **21**, 3094 (2011).
17. Y. G. Seo, H. Lee, K. Kim, and W. Lee, Mol. Cryst. Liq. Cryst. **520**, 201 (2010).
18. S. Kim, Y. G. Seo, Y. Cho, J. Shin, S. C. Gil, and W. Lee, Bull. Korean Chem. Soc. **31**, 1891 (2010).
19. S. C. Gil, Y. G. Seo, S. Kim, J. Shin, and W. Lee, Thin Solid Films **518**, 5731 (2010).